Chinese Chemical Letters 34 (2023) 107685

Contents lists available at ScienceDirect

Chinese Chemical Letters

journal homepage: www.elsevier.com/locate/cclet

Gadolinium-based contrast agents built of DO3A-pyridine scaffold: Precisely tuning carboxylate group for enhanced magnetic resonance imaging

Yongyin Geng[a,†], Tianze Wu[a,†], Qiuyue Han[b], Yongtai Yang[a], Zhenxia Chen[a], Xuanxuan Li[b], Bo Yin[b], Yaming Zhou[a], Yun Ling[a,*]

[a] Shanghai Key Laboratory of Molecular Catalysis and Innovative Materials, Department of Chemistry, Fudan University, Shanghai 200438, China
[b] Department of Radiology, Huashan Hospital North, Fudan University, Shanghai 201907, China

ARTICLE INFO

Article history:
Received 24 May 2022
Revised 15 June 2022
Accepted 15 July 2022
Available online 17 July 2022

Keywords:
Gadolinium-based contrast agents
Cyclen-based ligand
Structure-property relationship
Relaxivity
Magnetic resonance imaging

ABSTRACT

It is greatly desired to develop novel gadolinium-based contrast agents (GBCAs) as improved platforms for magnetic resonance imaging (MRI). Herein, we report the syntheses of a series of nonionic cyclen-based GBCAs by precisely tuning carboxylate group on DO3A-pyridine scaffold. [Gd-DO3A-4cp] is isolated which adopts an octadentate coordination mode with a free carboxylate group at 4-position of pyridine. It shows the r_1 relaxivity of 5.8 $(mmol/L)^{-1}$ s^{-1} (3 T, 25 °C), which is 75% higher than 3.3 $(mmol/L)^{-1}$ s^{-1} of the clinic used [Gd-DOTA]. The possible mechanisms behind the enhanced relaxivity are investigated and proposed by structure-property relationship studies. After validation of low cytotoxicity and considerable kinetic inertness, *in-vivo* studies are further examined, demonstrating its good MRI performance, biodistribution as well as the way of excretion.

Macrocyclic gadolinium-based contrast agents (GBCAs) generally refer to a class of Gd(III)-chelates built of twelve-membered cyclen ligands (cyclen = 1,4,7,10-tetraazacyclododecane) that can be used to reduce the longitudinal relaxation time (T_1) of protons in their vicinity for contrast-enhanced magnetic resonance imaging (MRI) [1,2]. Owing to the unique cyclen-based scaffold, they are more kinetically inert toward dissociation thus minimizing the risk of Gd(III) release [3–8], Nevertheless, they still suffer the low relaxivities. Ionic hyperosmolar [Gd-DOTA] is the agent clinically used. Despite its highest thermodynamic stability and kinetic inertness [9,10], its relaxivity is only slightly higher than 3 $(mmol/L)^{-1}$ s^{-1}. Though nonionic agents such as [Gd-HP-DO3A] and [Gd-DO3A-butrol] compensate the hyperosmolar issue, these GBCAs still encounter the relaxivities with the data smaller than 4 $(mmol/L)^{-1}$ s^{-1} [11].

Recent history has exemplified their developments. A promising strategy is to chemically graft them onto nanoparticles or macromolecules [12–14]. Despite the insurance of more rotational correlation time for relaxivity enhancement, this chemical grafting would lead a reduction of octadentate coordination sites provided by the cyclen ligands [15,16]. This reduction has been revealed to compromise the thermodynamic and/or kinetic stability of cyclen-based GBCAs [17], which would inevitably raise the concerns of Gd^{3+} release though an enhanced sensitivity for recognizing molecule signatures within the disease pathologies along the way of chemical grafting could be expected. Therefore, structurally overcoming this issue is further fundamentally desired. Another feasible strategy is to facilitate the exchange rate of water between inner and second sphere of cyclen-based GBCAs [18–22]. Introducing bulky groups onto either cyclen-ring [23] or α-position of the acetate pendant arm [24,25] or replacing the pendant arm [22,26] is proved to be a way for the faster water-exchange since it renders the capped twisted-square antiprismatic (TSAP) over capped square antiprismatic (SAP) isomer of GBCAs in aqueous solution. Despite the observable progress, the relaxivity is still around 4 $(mmol/L)^{-1}$ s^{-1} [27].

In view of the above issues, in this work, we present our studies on the pendant arm (Scheme 1). The idea could be viewed as replacing one acetate of DOTA with pyridine while leaving the hydrophilic carboxylate on pyridine tuned for the relaxivity as well as reserved as a reactive group for potential grafting. Here, we report the syntheses and the screening of nonionic [Gd-DO3A-4cp]. It shows an optimal r_1 relaxivity of 5.8 $(mmol/L)^{-1}$ s^{-1} (3 T, 25 °C)

* Corresponding author.
E-mail address: yunling@fudan.edu.cn (Y. Ling).
† These authors contribution equally to this work.

https://doi.org/10.1016/j.cclet.2022.07.028
1001-8417/

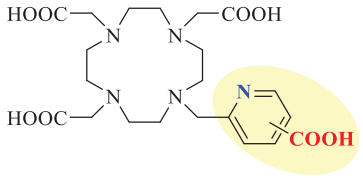

COOH position	Derivatives
\	DO3A-pyr
ortho	DO3A-6cp
meta	DO3A-5cp
para	DO3A-4cp

Scheme 1. Cyclen-based ligands of the DO3A-pyridine scaffold.

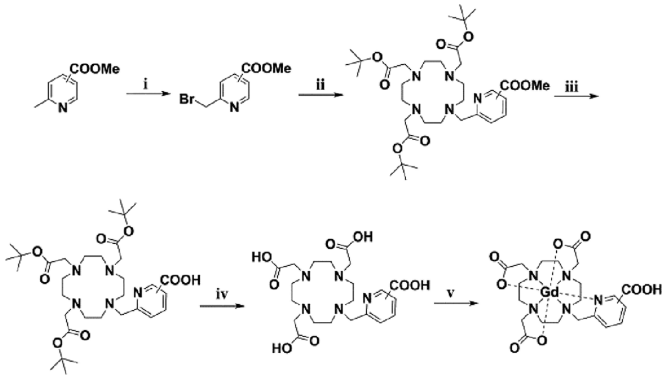

Fig. 1. Protection-derivatization-deprotection protocol for the synthesis of DO3A-pyridine derivatives as well as the corresponding GBCAs. Reagents and conditions: (i) NBS, BPO, CCl_4, r.t., 12 h, (ii) DO3A-tBu$_3$, K_2CO_3, MeCN, 50 °C, 12 h, (iii) NaOH, H_2O, Dioxane, r.t., 12 h, (iv) TFA, CH_2Cl_2, r.t., 12 h, (v) $GdCl_3{\cdot}6H_2O$, pH 6∼7, r.t., 12 h.

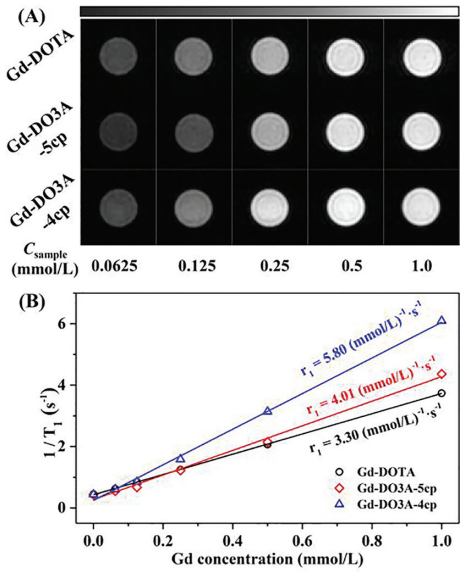

Fig. 2. Relaxivity (r_1) measurements for Gd-DOTA, Gd-DO3A-5cp and Gd-DO3A-4cp at 3.0 T and 25 °C, (A) Phantom images and (B) plots of r_1 at various concentrations.

Table 1
The relaxivity of Gd-DOTA and Gd-DO3A-pyridine derivatives and log*P* estimated by HPLC method.

Complex	r_1 [(mmol/L)$^{-1}$ s^{-1}]		log*P*
	0.5 T (32 °C)	3.0 T (25 °C)	
Gd-DOTA	3.00 ± 0.03	3.30 ± 0.02	N.A.
Gd-DO3A-pyr	2.27 ± 0.01	2.49 ± 0.01	−0.65
Gd-DO3A-6cp	1.23 ± 0.01	1.25 ± 0.01	−1.70
Gd-DO3A-5cp	3.46 ± 0.21	4.01 ± 0.15	−1.77
Gd-DO3A-4cp	5.49 ± 0.26	5.80 ± 0.15	−1.72

that significantly transcends 3.3 (mmol/L)$^{-1}$ s^{-1} of clinic used [Gd-DOTA]. Structure-property relationship studies reveal the possible mechanisms which are associated with the increased ratio of TSAP over SAP isomers as well as the presence of hydrophilic carboxylate group. Given the verified low cytotoxicity and kinetic inertness toward transmetallation, *in-vivo* whole-body MRI on mice is further examined and compared with [Gd-DOTA] demonstrating the favored performance as well as biodistribution and excretion profiles. These results suggest that it could service as an improved platform for further MRI studies.

The DO3A-pyridine derivatives were obtained by the protection-derivatization-deprotection synthetic procedures presented in Fig. 1. Generally, the alkylation reaction of *t*-Bu$_3$DO3A with bromomethylpyridine derivatives at room temperature gave rise to the formation of corresponding *t*-Bu$_3$DO3A-pyridine compounds. After the purification and removal of ester groups by hydrolysis, it resulted into the isolation of corresponding macrocyclic ligands (Figs. S1-S12 in Supporting information). It should be mentioned that complete deprotection was achieved by treatment of aqueous solution of sodium hydroxide. Treated by trifluoroacetic acid, it only led to the hydrolysis of *tert*–butyl acetate. Corresponding lanthanide(III) chelates were subsequently prepared in aqueous solution at room temperature under pH value of 6∼7 overnight and purified by RP C18-silica (Figs. S13-S16 in Supporting information). HPLC analyses confirmed the generation of corresponding chelate compounds and HRMS spectra identified the molecular weight in accordance with expected one.

MRI performance of the isolated Gd chelates was *in-vitro* evaluated on a 0.5 and 3 T scanner respectively. Similar to the control group of commercially available [Gd-DOTA], a brightening trend of T_1-weighted images was observed as the increase of concentration, in which [Gd-DO3A-4cp] and [Gd-DO3A-5cp] were distinguished themselves (Fig. 2). To quantitatively assess the MRI enhancement, the longitudinal (r_1) relaxivity was then obtained by fitting the relaxation rate as a function of the concentration respectively. All data were deposited in Table 1. [Gd-DO3A-pyr] exhibited a r_1 value of 2.49 (mmol/L)$^{-1}$ s^{-1} (3.0 T, 25 °C), which is slightly lower than 3.3 (mmol/L)$^{-1}$ s^{-1} for [Gd-DOTA]. However, carboxylation of the pyridine group of [Gd-DO3A-pyr] at 6-position led to a decrease of r_1 to 1.25 (mmol/L)$^{-1}$ s^{-1} in [Gd-DO3A-6cp]. Despite this, further shifting the carboxylate group from 6 to 5- and 4-position revealed an enhancement of r_1 with the value of 4.01 and 5.8 (mmol/L)$^{-1}$ s^{-1} for [Gd-DO3A-5cp] and [Gd-DO3A-4cp] respectively, which is 25% and 75% higher than that of [Gd-DOTA]. In addition, a similar trend was also confirmed at 0.5 T and 32 °C (Fig. S17 in Supporting information).

To reveal the structure-dependent MRI contrast, we firstly evaluated the hydrophilicity using the octanol–water partition coefficient (log*P*) obtained by HPLC (Fig. S18 and Table S1 in Supporting information). As shown in Table 1, the lower log*P* value revealed the hydrophilic enhancement by carboxylation of pyridine group, which implies more water molecules would be involved in the second coordination sphere of Gd chelates [28,29]. Thus, according to the SBM equation [30,31], a higher r_1 value could be expected, except for [Gd-DO3A-6cp] where a smallest r_1 was observed. This exception should be ascribed to the replacement of capped water molecule by the carboxylate group in the capped square-antiprismatic coordinated geometry of Gd(III), resulting into none water molecule in the inner sphere [32]. In contrast, the

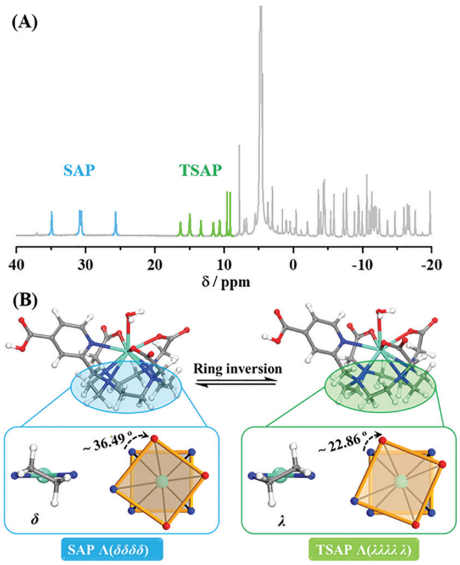

Fig. 3. (A) ^{1}H NMR spectra of [Eu(DO3A-4cp)(D_2O)] in D_2O solution, the signals of cyclen protons used for ^{1}H 1D-EXSY studies are highlighted in blue (SAP axial protons), green (TSAP axial protons). (B) Calculated isomers of [Gd-DO3A-4cp] in which it shows the detailed macrocyclic fragment changes as well as the average angle of rotation between the N_4 and O_3N_1 planes.

inner sphere hydration number (q) of [Gd-DO3A-5cp] and [Gd-DO3A-4cp] was estimated to be 1.05 and 1.08 respectively according to the empirical expression reported by Horrocks and Sudnick (Fig. S19 in Supporting information) [33]. We have tried to isolate their crystal structures to confirm the water molecule in the inner and secondary sphere but failed. Nevertheless, single crystal X-ray diffraction study on an analogue of [Gd-DO3A-5cp], a methyl ester compound formulated as [Gd-DO3A-5cpm] (Figs. S20-S24 and Table S2 in Supporting information), confirmed the presence of one coordinated water molecule and water clusters in the inner and secondary sphere respectively. In this context, compared with [Gd-DOTA], the enhancement of MRI contrast of [Gd-DO3A-5cp] and [Gd-DO3A-4cp] could be ascribed to the faster water-exchange rate between the inner and second coordination sphere as they have the same hydration number, similar hydrophilic nature and paramagnetic properties.

Water-exchange rate is an important parameter positively associated with the T_1-weighted MRI [34]. For macrocyclic MRI contrast agents, this parameter is structurally related to the relative populations of Gd(III) conformational isomers in the aqueous solution, which are commonly classified into square-antiprismatic (SAP) and twisted square antiprismatic (TSAP) conformations defined by the torsion angle of two coordination planes [35]. TSAP isomer facilitates the water exchange leading to the enhancement of MRI. Therefore, ^{1}H NMR spectroscopy was consequently used to distinguish the SAP and TSAP based on the corresponding surrogate Eu(III) complexes (Fig. 3 and Figs. S25-S27 in Supporting information). The observation of chemical shifts in range of 25–40 ppm (assigned to four predominant axial ring protons) demonstrated the presence of SAP isomer [22]. Integration of the signals assigned to TSAP and SAP for the equilibrium reaction of TSAP↔SAP yielded the constant $K_{integral}$ of 0.44 and 0.54 for [Eu-DO3A-5cp] and [Eu-DO3A-4cp] respectively, which is higher than that of 0.21 for [Eu-DOTA] (surrogate model for [Gd-DOTA]) [36], suggesting more favored TSAP isomer in aqueous solution. To further gain insight into the mechanisms, DFT studies were consequently performed. Geometrically optimized structures using solvent (water) model provided the expected TSAP and SAP isomers (Fig. 3B), in which the calculated average torsion angle of TSAP isomer is about 23.22° and 22.86° respectively for [Gd-DO3A-5cp] and [Gd-DO3A-4cp], and the torsion angle of SAP isomer is about 36.24° and 36.49° assigned for [Gd-DO3A-5cp] and [Gd-DO3A-4cp] respectively. Further considering the SAP ↔ TSAP kinetic process, their Gibbs free energies were calculated, revealing a lower energy in TSAP isomer for both [Gd-DO3A-5cp] and [Gd-DO3A-4cp] (Table 2). The favored TSAP isomer could be ascribed to the bulky pyridine pendant arm on the cyclen-ring [37,38].

Given the enhanced relaxivity, *in-vivo* MRI evaluation was consequently carried out. Prior to the study, *in-vitro* cytotoxicity was respectively estimated on HepG2 and A549 cell lines by Cell Counting Kit-8 (Figs. 4A and B). The cell viability remained around 100% as the increase of concentration even at 1000 μmol/L, indicating that both [Gd-DO3A-5cp] and [Gd-DO3A-4cp] have no obvious cytotoxicity similar to the control group of [Gd-DOTA]. Transmetallation of [Gd-DO3A-5cp] and [Gd-DO3A-4cp] was also respectively studied to assess the kinetic stability of the scaffold in the presence of Zn(II) ion [39,40]. The evolution of normalized paramagnetic relaxation rate $R_1^P(t)/R_1^P(0)$ at a given time remained steady (Fig. 4C), demonstrating the satisfied kinetic stability to prevent the *in-vivo* transmetallation. In this context, the *in-vivo* study was performed on a 3.0 T system. The coronal T_1-weighted whole-body MR images displayed the biodistribution and excretion after administration (Fig. 4D). Compared to [Gd-DOTA], the overall contrast enhancements were observed by [Gd-DO3A-5cp] and [Gd-DO3A-4cp] at liver after injection, which displayed 22.3% and 31.9% enhancement at 30 min post-injection and then signals decreased as the increase of time (Fig. 4E). Similar processes were also observed at kidney (Fig. S28 in Supporting information). These results demonstrated their considerable *in-vivo* MRI capabilities. The major organs (heart, liver, spleen, lung, kidney) were then stripped and stained with hematoxylin and eosin (H&E, Fig. S29 in Supporting information). Compared with the [Gd-DOTA] group, there was no obvious tissue damage and apparent histopathological abnormality, indicating their good biocompatibilities.

In conclusion, studies on the pyridine pendant arm based on a DO3A-pyridine scaffold were presented. The nonionic [Gd-DO3A-4cp] shows an optimal relaxivity, low cytotoxicity and considerable kinetic inertness, rendering it more favored *in-vivo* MRI profiles as compared with [Gd-DOTA]. In addition, its pre-reserved carboxylate group also structurally paves the way for potential chemical grafting. Our studying results not only provide a novel cyclen-based GBCA with the promise as an ideal platform, but also vividly

Table 2
The paraments of theoretical calculation of TSAP and SAP isomers.

Paraments	[Gd-DO3A-4cp]		[Gd-DO3A-5cp]	
	SAP	TSAP	SAP	TSAP
E_{total} (kcal/mol)	−7,903,201.261	−7,903,203.752	−7,903,202.542	−7,903,203.929
$G_{total}^{298.15\ K}$ (kcal/mol)	281.671	281.264	282.73	281.164
$E_{Tcorr}^{298.15\ K} = E_{total} + G_{total}$	−7,902,919.590	−7,902,922.488	−7,902,919.812	−7,902,922.765
$\Delta G^{298.15\ K}$		−2.898		−2.954

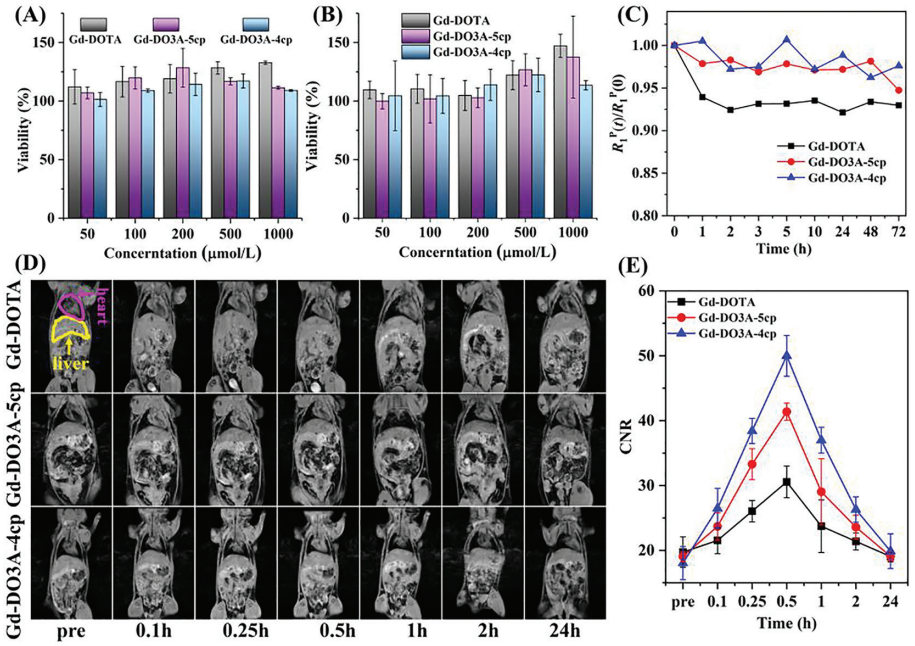

Fig. 4. Cell viability of (A) HepG2 and (B) A549 incubated with Gd-DOTA, Gd-DO3A-5cp and Gd-DO3A-4cp. (C) Evolution of the relative water proton paramagnetic longitudinal relaxation rate $R_1^P(t)/R_1^P(0)$ *versus* time (from 0 to 72 h) for Gd-DOTA, Gd-DO3A-5cp, and Gd-DO3A-4cp. (D) SPGR-T1WI of normal mice acquired before (pre) and 0.1, 0.25, 0.5, 1, 2 and 24 h after tail vein injection of Gd-DOTA, Gd-DO3A-5cp or Gd-DO3A-4cp at a dose of 0.1 mmol/kg by using 3.0 T MRI. (E) Contrast-to-noise ratio (CNR) time course in the liver.

portray a practicable way to the developments of more efficient GBCAs.

Notes

The animal protocol was approved by the Experimental Animal Management and Ethics Committee at the School of Basic Medical Sciences, Fudan University.

Declaration of competing interest

The authors declare that they have no known competing financial interests or personal relationships that could have appeared to influence the work reported in this paper.

Acknowledgments

We gratefully acknowledge the financial support from National Natural Science Foundation of China (No. 21971045), National Key Technologies R&D Program of China (No. 2017YFA0205103).

Supplementary materials

Supplementary material associated with this article can be found, in the online version, at doi:10.1016/j.cclet.2022.07.028.

References

[1] J. Wahsner, E.M. Gale, A. Rodríguez-Rodríguez, P. Caravan, Chem. Rev. 119 (2019) 957–1057.
[2] H. Dong, S.R. Du, X.Y. Zheng, et al., Chem. Rev. 115 (2015) 10725–10815.
[3] L. Yang, I. Krefting, A. Gorovets, et al., Radiology 265 (2012) 248–253.
[4] T. Kanda, K. Ishii, H. Kawaguchi, K. Kitajima, D. Takenaka, Radiology 270 (2014) 834–841.
[5] R.J. McDonald, J.S. McDonald, D.F. Kallmes, et al., Radiology 275 (2015) 772–782.
[6] E. Kanal, M.F. Tweedle, Radiology 275 (2015) 630–634.
[7] I.A. Dekkers, R. Roos, A.J. van der Molen, Eur. Radiol. 28 (2018) 1579–1584.
[8] J. Ramalho, R.C. Semelka, M. Ramalho, et al., Am. J. Neuroradiol. 37 (2016) 1192–1198.
[9] M. Port, J.M. Idée, C. Medina, et al., BioMetals 21 (2008) 469–490.
[10] E.M. Gale, P. Caravan, A.G. Rao, et al., Pediatr. Radiol. 47 (2017) 507–521.
[11] L.M. De León-Rodríguez, A.F. Martins, M.C. Pinho, N.M. Rofsky, A.D. Sherry, J. Magn. Reson. Imaging 42 (2015) 545–565.
[12] C.H. Huang, A. Tsourkas, Curr. Top. Med. Chem. 13 (2013) 411–421.
[13] Z. Zhou, M. Qutaish, Z. Han, et al., Nat. Commun. 6 (2015) 7984.
[14] S.D. Foillard, A. Billet, R.M. Dubuisson, et al., Bioconjug. Chem. 33 (2022) 180–193.
[15] G. Gambino, T. Gambino, L. Connah, et al., J. Med. Chem. 64 (2021) 7565–7574.
[16] R.J. Holbrook, N. Rammohan, M.W. Rotz, et al., Nano Lett. 16 (2016) 3202–3209.
[17] P. Caravan, Chem. Soc. Rev. 35 (2006) 512–523.
[18] T.J. Clough, L.J. Jiang, K.L. Wong, N.J. Long, Nat. Commun. 10 (2019) 1420.
[19] P. Hermann, J. Kotek, V. Kubíček, I. Lukeš, Dalton Trans. (2008) 3027–3047.
[20] B.N. Siriwardena-Mahanama, M.J. Allen, Molecules 18 (2013) 9352–9381.
[21] P. Caravan, D. Esteban-Gómez, A. Rodríguez-Rodríguez, I. Platas-Iglesias, Dalton Trans. 48 (2019) 11161–11180.
[22] L. Leone, D. Esteban-Gómez, C. Platas-Iglesias, M. Milanesio, L. Tei, Chem. Commun. 55 (2019) 513–516.
[23] L.X. Dai, C.M. Jones, W.T.K. Chan, et al., Nat. Commun. 9 (2018) 857.
[24] E.C. Wiener, M.C. Abadjian, R. Sengar, et al., Inorg. Chem. 53 (2014) 6554–6568.
[25] A.F. Mingo, S.C. Serra, S. Baroni, et al., Magn. Reson. Med. 78 (2017) 1523–1532.
[26] M. Polášek, M. Šedinová, J. Kotek, et al., Inorg. Chem. 48 (2009) 455–465.
[27] L.R. Tear, C. Carrera, E. Gianolio, S. Aime, Chem. Eur. J. 26 (2020) 6056–6063.
[28] C.S. Bonnet, P.H. Fries, S. Crouzy, et al., Chem Eur. J. 15 (2009) 7083–7093.
[29] M.W. Rotz, K.S.B. Culver, G. Parigi, et al., ACS Nano 9 (2015) 3385–3396.
[30] K.Y. Ni, Z.H. Zhao, Z.J. Zhang, et al., Nanoscale 8 (2016) 3768–3774.
[31] C. Richard, B.T. Doan, J.C. Beloeil, et al., Nano Lett. 8 (2008) 232–236.
[32] E.E. Racow, J.J. Kreinbihl, A.G. Cosby, et al., J. Am. Chem. Soc. 141 (2019) 14650–14660.
[33] W. Horrocks, D.R. Sudnick, J. Am. Chem. Soc. 101 (1979) 334–340.
[34] A.D. Sherry, Y.K. Wu, Curr. Opin. Chem. Biol. 17 (2013) 167–174.
[35] G. Tircso, B.C. Webber, B.E. Kucera, V.G. Young, M. Woods, Inorg. Chem. 50 (2011) 7966–7979.
[36] J. Blahut, P. Hermann, Z. Tošner, C.P. Iglesias, Phys. Chem. Chem. Phys. 19 (2017) 26662–26671.
[37] M. Milne, M. Lewis, N. McVicar, et al., RSC Adv. 4 (2014) 1666–1674.
[38] M. Woods, M. Botta, S. Avedano, J. Wang, A.D. Sherry, Dalton Trans. (2005) 3829–3837.
[39] A.R. Baek, H.K. Kim, S. Park, et al., J. Med. Chem. 60 (2017) 4861–4868.
[40] L. Bian, M. Gao, D. Zhang, et al., Anal. Chem. 90 (2018) 13249–13256.